Applied Thermal Engineering 234 (2023) 121183

Contents lists available at ScienceDirect

Applied Thermal Engineering

journal homepage: www.elsevier.com/locate/apthermeng

Research Paper

Indoor experimental analysis of Serpentine-Based cooling scheme for high concentration photovoltaic thermal systems

William J. Cameron [a,*], Mussad M. Alzahrani [b], James Yule [a], Katie Shanks [a], K.S. Reddy [c], Tapas K. Mallick [a]

[a] Environment and Sustainability Institute, University of Exeter, Penryn Campus, Cornwall, TR10 9FE, UK
[b] Mechanical and Energy Engineering Department, Imam Abdulrahman Bin Faisal University, Dammam, 34212, Saudi Arabia
[c] Heat Transfer and Thermal Power Laboratory, Department of Mechanical Engineering, Indian Institute of Technology Madras, Chennai, 600 036, India

ARTICLE INFO

Keywords:
High concentrator photovoltaic
Heat sink
Multi-junction solar cell
Exergy efficiency
Photovoltaic thermal hybrid
Ray tracing

ABSTRACT

High concentration photovoltaic thermal hybrids are expected to play an important role in meeting growing energy demands. When approaching concentrations over 1000 suns, a cooling system is needed to maximise both the thermal and electrical performance of the multi-junction solar cell without producing excessive parasitic losses.

This study develops a novel simulation model to provide an in-depth understanding of the functionality of a concentrated photovoltaic thermal hybrid system with serpentine-based cooling systems. An ultra-high concentrator photovoltaic optic irradiance profile (peak effective concentration ratio: ~1500 suns) is considered within the simulation model, which has been validated through indoor experimentation. The effectiveness of cooling is also evaluated through maximum thermal stresses generated in the multi-junction solar cell. The double serpentine design was deemed the highest performing, primarily because of the single serpentine's excessive pressure drop. Copper as the heat sink material yielded superior performance because of its higher thermal conductivity. The maximum total exergetic efficiency achieved by the receiver was ~ 10.9% with this configuration. Compared to some examples in the literature this value may seem low, however, it is more accurate due to the inclusion of a specific irradiance profile. All serpentine-based cooling systems could maintain the recommended operating temperature.

1. Introduction

With a growing interest in renewable energy, it is vital to improve the performance and applicability of renewable energy generators. The use of concentrated photovoltaic thermal (CPV/T) hybrids has a lot of potential in this area. The use of relatively cheap optics to focus light onto more expensive, and more efficient multi-junction (MJ) solar cells can yield higher electricity production. The consequential heat flux caused by the intense solar irradiance can be extracted for later application, further improving the potential of the system. As CPV/T technology reaches ultra-high (UH) concentrations, highly effective cooling systems are needed which can maintain somewhat uniform temperature profiles whilst maximising the waste heat capture. Pairing a serpentine-based cooling geometry with a high concentration 5.5 × 5.5 mm^2 MJ solar cell can lead to new records in concentrated photovoltaic (CPV) systems power outputs without substantial detriment to system lifetime. From a previous literature review, cooling systems with centralised inlets are the most promising for point focused systems [1,2]. Previous researchers have suggested that solar cells under concentrations greater than 400 suns can reach temperatures substantially higher than recommended for operation (greater than110 ℃) with no heat sink [3,4].

Ahmed et al. [5] conducted a theoretical investigation into the effectiveness of serpentine cooling schemes for MJ cells under high concentration, specifically the side inlet serpentine and the central inlet serpentine. It was found that the central inlet serpentine was superior and showed higher exergetic efficiencies. The power input is set as a uniform heat source within the germanium layer of the solar cell. The manufacture tolerance is 0.5 mm throughout the channels. Pumping power is excessive due to the long flow path. At 1500 suns, the solar cell

Abbreviations: CPV/T, Concentrated photovoltaic/thermal; MJ, Multi-junction; UH, Ultra-high; CPV, Concentrated photovoltaic; SS, Single serpentine; DS, Double serpentine; HTF, Heat transfer fluid; DNI, Direct normal irradiance.

* Corresponding author.
E-mail address: wc303@exeter.ac.uk (W.J. Cameron).

https://doi.org/10.1016/j.applthermaleng.2023.121183
Received 14 July 2022; Received in revised form 17 May 2023; Accepted 16 July 2023
Available online 22 July 2023

Nomenclature

H	Height
R	Radius
d/D	Diameter
d	Depth
t	Thickness
L	Length
W	Width
Al	Aluminium
Cu	Copper
η	Efficiency
ln	Natural logarithm
I	Short circuit current
C	Concentration factor
β	Temperature coefficient
ρ	Density
cp	specific heat capacity
k	Thermal conductivity
μ	Dynamic Viscosity
T	Temperature
P	Power
A	Area
$\dot{Q}$	Energy rate
ΔT	Change in temperature
R	Resistance
E	Exergy
ξ	Exergetic efficiency
E	Young's modulus
ν	Poisson's ratio
α	Coefficient of thermal expansion
$\dot{V}$	Volumetric Flow rate
p	Pressure drop
$\dot{m}$	Mass flow rate

Subscripts

ch	Channel
wall	Wall
in	Inflow
out	Outflow
cell	Relating to solar cell
top	Top
ref	reference
sc	Solar cell
opt	optical
heat	Thermal
max	Maximum
min	Minimum
f	Fluid
pump	Pump
tot	total
sys	System
elec	Electrical
sun/s	Solar
a	Ambient
eff	Effective
conc	Under concentration
bare	Not under concentration (normal irradiance)

efficiency reached 35.7% and the total system exegetic efficiency reached 35.0% when modelled with uniform irradiance. Alamri et al. [6,7] combined COMSOL Multiphysics' *Ray Optics* and *Heat Transfer in Solids and Fluids* physics packages. The cooling system is simple as the focus is placed on the ray tracing section. No exergetic efficiency is calculated, however, the thermal energy is applied to an organic Rankine cycle. Coupling physics packages directly in COMSOL suggests the heat generated is a flux over the surface of the cell, rather than a volumetric heat source which is preferred. Electrical efficiencies vary between 38.8 and 39.3% under a geometric concentration ratio of 400 suns. Gao et al. [8] simulated and experimentally validated a low concentration (4 suns) CPV/T with a non-MJ bifacial solar cell, an exergy analysis is also included. The heat sink has a central inlet, but the geometry has a relatively small convective heat transfer area, meaning it would likely not yield good performance at higher concentration ratios. Hamdy et al. [9] conducted an exergoeconomic investigation for a parabolic trough solar collector and found that high exergy outputs yielded the most economic system, unless there is a large difference in investment cost. Felsberger et al. [20] found low electrical efficiencies at first but found that calibration of the optic and cell position gave a boost from the feasibility test. Several studies have used the uniform heat source germanium approach within the literature [10–16], others have approximated using gaussian distribution [17,18], few have used coupled ray tracing. Uniform heat sources neglect heat generated by irradiance peaks which are vital considerations for heat sink design. Gaussian distributions are much easier to model in comparison to irradiance distributions based on ray tracing, it is important to compare these options and the resultant error each cause. It is important to link the irradiance distribution to the heat flux to precisely design microchannel geometry through computational thermo-fluid dynamics. Removal of broad assumptions leads to more realistic performance indicators, particularly lower efficiency values. Studies with theoretical focus need to use experimental data for validation to ensure accuracy, preferably this will be specific to the experimental set up as in [19–21]. When this is not possible, several studies use literature data to validate the model when set to the same boundary conditions ([22,23]), although this adds less certainty. Papis-Frączek and Sornek [2] warned against directly comparing efficiency values for actively cooled CPV/Ts due to the misleading effect of different operating conditions.

The objective of the present study is, firstly, to understand the influence on the performance of a CPV/T with a peak concentration ratio up to ~ 1500 suns equipped with various serpentine-based cooling schemes. For this study, serpentine cooling systems consist of central inlet microchannels which spiral outwards from the centre of the heat sink. These can maximise the heat transfer area between fluid and metal while introducing the lowest temperature section of the fluid to the point of maximum heat flux. Thus, guaranteeing a high heat transfer rate. Single and double configurations are included, where the name of the configuration describes the number of flow paths within the channels. Secondly, considering each part of the CPV/T, and integrating optical simulation through ray tracing to electrical power and heat generation, allowed the creation of a thorough simulation method which has been experimentally validated. The novelty of this study is found in the specific design of the heat sinks presented, the validation of the simulation method, and the evaluation of the performance and specific UH concentration conditions. The full system simulative model is used to explore the effect of the heat sink configurations, mass flow rate, and irradiance profile on different performance indicators. These include: the maximum solar cell temperature, cell temperature non-uniformity, thermal stress generation, as well as the electrical and thermal energy and exergy efficiencies.

2. Physical model and theoretical approaches

2.1. Physical models

Building on the original serpentine cooling scheme by Ahmed et al. [5], new designs have been developed with notable changes. Firstly, all designs have been scaled to an AZURE SPACE 5.5 × 5.5 mm^2 MJ-CPV cell ADDIN CSL_CITATION [24] rather than the 10 mm^2 CPV cell used in the original system. Secondly, the expected concentration ratios and illumination profiles are based on specific optical systems rather than scaled volumetric energy inputs. The manufacture tolerance has been changed to make construction easier. In this case the channel width is 1 mm, but the channel walls remain 0.5 mm. From the literature it is clear that maximising the convective heat transfer area is beneficial to promote cooling ability. Generally, this is achieved by maximising the number of channels and minimising the thickness of channel walls. Hence, the manufacture tolerance is chosen to produce the smallest channels without needing highly specialised equipment. The dimensions are detailed in Table 1 and Table 2. Additionally, two heat sink materials are evaluated. Namely, aluminium, which is used in the original proposal, and copper. Material properties are shown in Table 3, data from [15]. The schematic diagrams of the proposed heat sinks are presented in Fig. 1 and Fig. 2.

The original single channelled central inlet serpentine has been converted into the single serpentine (SS), to counter the dead-zone of fluid flow observed in the central cavity, a double serpentine (DS) has been proposed. The DS shortens the flow path length which reduces the pressure drop as well as the average fluid temperature. Both designs can be seen in Fig. 1. Corner holes without countersink attach to fasteners which hold the CPV cell module in place. The inlet for the heat transfer fluid (HTF) is directly beneath the cell, as is shown in Fig. 2. The same dimensions are used in both, where applicable. The depth of the slot for the solar cell within the top heat sink layer is half the depth of the bottom two layers of the solar cell circuit board, to prevent short circuiting and to maintain the cell position. The flow rate is evaluated in the laminar range for each cooling system geometry where the temperature profile converges, between 40 and 300 g/min. The SS heat sink's maximum flow rate is 250 g/min due to the substantial pressure drop, which limited the flow range during experimentation.

Two concentrator optics are investigated. A 21 cm^2 square Fresnel lens with an optimal focal length of 43 cm, where the material, silicon-on-glass, has a refractive index of 1.45. An UH concentration irradiance profile is simulated based on the UH-CPV optic developed by the University of Exeter's solar energy research group [25]. The optimal focal image of each optic is used. The indoor experimental analysis is used to validate the theoretical model, outdoor conditions are then estimated using this methodology.

Table 1
Dimensions of various layers of the CPV/T.

Layer	Width (mm)	Length (mm)	Thickness (mm)
GaInP	5.5	5.5	0.07
GaInAs	5.5	5.5	0.07
Ge	5.5	5.5	0.07
Copper-I	15.0	16.6	0.25
Al_2O_3-Ceramic	18.0	19.6	0.32
Copper-II	18.0	19.6	0.25
Thermal Paste	18.0	19.6	0.30
Heat sink (Top plate)	36.0	36.0	4.8
Heat sink (Bottom plate)	36.0	36.0	3.0

Table 2
Detailed dimensions of cooling system geometries.

Parameter	Value (mm)	Parameter	Value (mm)
H_{ch}	3.0	R_{ch}	0.5
d_{in}	2.0	R_{wall}	0.4
$d_{in,2}$	4.0	W_{out}	3.0
W_{ch}	1.0	d_{out}	2.0
t_{ch}	0.5	L_{in-ch}	2.5
L_{top-ch}	1.5	d_{cell}	0.3

Table 3
Material thermophysical properties of the CPV/T.

Material	Specific heat (J/kgK)	Thermal conductivity (W/mK)	Density (kg/m^3)	Emissivity
GaInP	370	73	4470	0.9
GaInAs	550	65	5316	–
Ge	320	60	5323	–
Copper	385	400	8700	0.05
Al_2O_3-Ceramic	900	27	3900	0.75
Aluminium	900	160	2700	0.05
Thermal Paste	800	10	4000	–

2.2. Mathematical approach

This mathematical model uses an iterative solver with the generalised residual method at tolerance 10^3 in COMSOL 5.6. The electrical efficiency is based on the cell temperature and the reference efficiency for a concentration ratio. The reference efficiency value as a function of concentration can be roughly represented by a second-degree polynomial, the effect of the temperature is linear and can be added leading to the following equation:

$$\eta_{sc} = -0.0000023C^2 + 0.00323354C + 41.42 - \left(\beta_{ref}(T_{sc} - 25)\right) \quad (1)$$

Where β_{ref} is 0.046% for the 2014 AZUR SPACE 5.5 × 5.5 mm^2 solar cell ADDIN CSL_CITATION {"citationItems":[{"id":"ITEM-1","itemData":{"abstract":"Sun Concentration Isc [A] Voc [V] IMPP [A] VMPP [V] PMPP [WMPP] FF [%] Ƞ [%] Version MC/Air Grid optimized for medium concentration + Antireflective Coating adapted to air X 250 Sun Concentration Isc [A] Voc [V] IMPP [A] VMPP [V] PMPP [WMPP] FF [%] Ƞ [%]","author":[{"dropping-particle":"","family":"AzurSpace","given":"","non-dropping-particle":"","parse-names":false,"suffix":""}],"id":"ITEM-1","issued":{"date-parts":[["2014"]]},"title":"Enhanced Fresnel Assembly-EFA Type: 3C42A-with 5,5x5,5mm^2 CPV TJ Solar Cell Application: Concentrating Photovoltaic (CPV) Modules Typical Average Electrical Data","type":"article-journal"},"uris":["https://www.mendeley.com/documents/?uuid = b7043ad0-7f7b-3f07-bbb7-df409f8e383f"]}],"mendeley":{"formattedCitation":"[24]","plainTextFormattedCitation":"[24]","previouslyFormattedCitation":"[23]"},"properties":{"noteIndex":0},"schema":"https://github.com/citation-style-language/schema/raw/master/csl-citation.json"}[24]. The efficiency across concentration and temperature can be seen in Fig. 3. This is used to predict the performance of the solar cell at concentration ratios where no experimental data is available.

The following assumptions are made within the theoretical model:

- Heat is generated in the germanium layer of the cell [26]. Light incident on the non-photovoltaic surface directly generates a heat flux.
- Physical properties of the HTF (water) vary with temperature as in the following equations (where T_f is in K) [14]:

$$\rho(kg/m^3) = -0.003T_f^2 + 1.505T_f + 816.781 \quad (2)$$

$$cp_f(J/kgK) = -0.0000463T_f^3 + 0.0552T_f^2 - 20.86T_f + 6719.637 \quad (3)$$

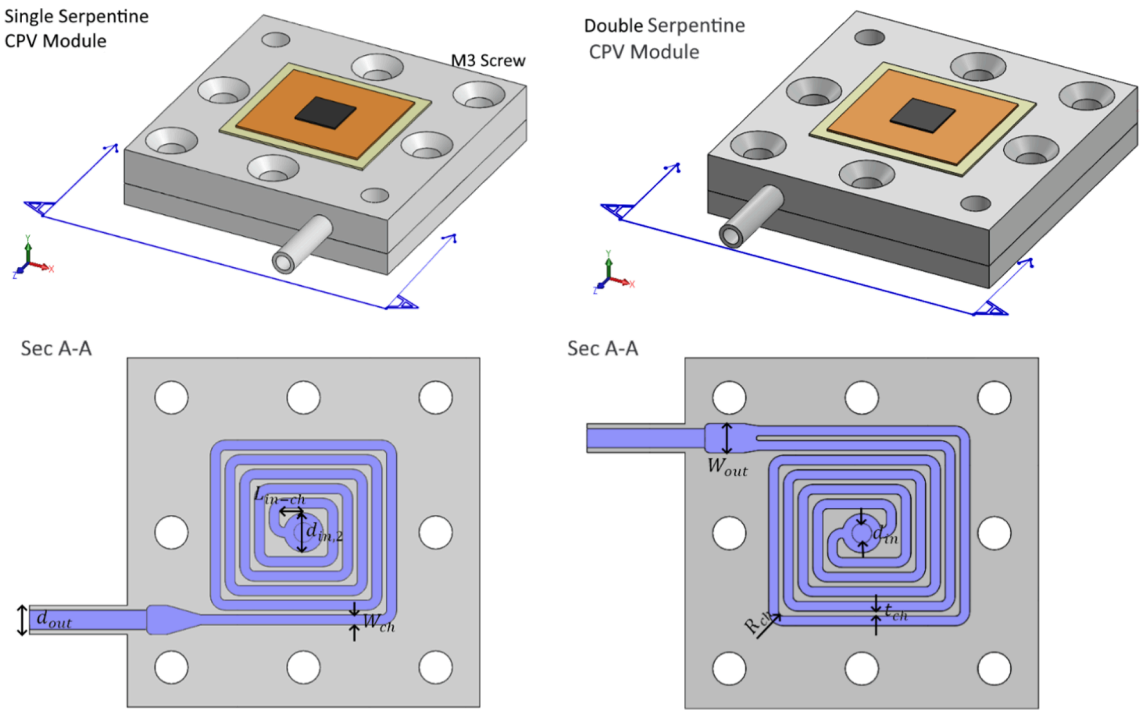

Fig. 1. Single serpentine CPV/T module (left), and double serpentine CPV/T module (right).

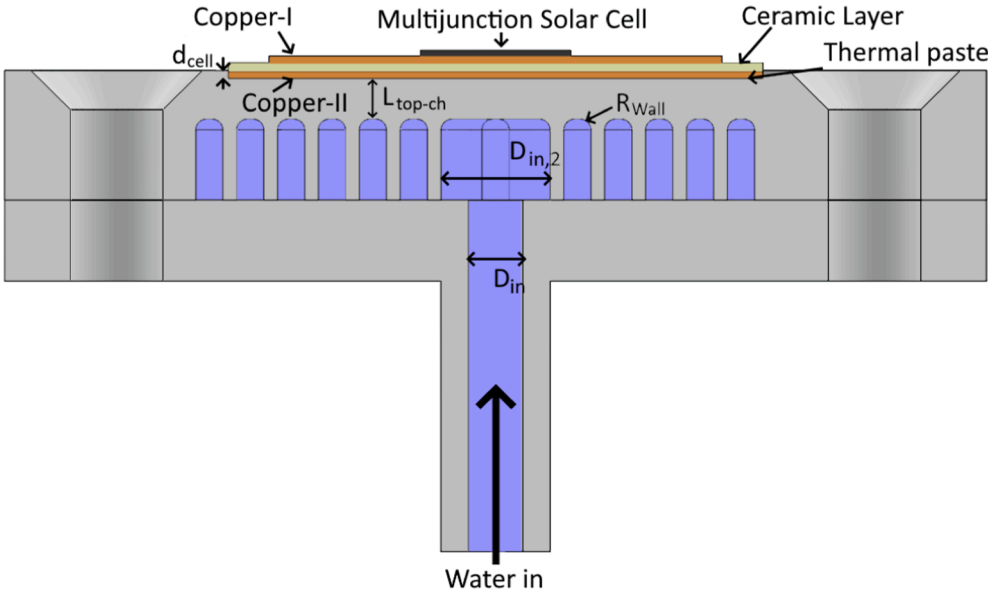

Fig. 2. Vertical (X-Y) cross section through the centre of the double serpentine module.

$$k_f(W/mK) = -0.0000078437T_f^2 + 0.0062T_f - 0.54 \quad (4)$$

$$\mu_f(Pas) = 0.00002414 \times 10^{(247.8/T_f - 140)} \quad (5)$$

- Natural convection and radiative heat losses are considered over all exposed surfaces of the module. Convective heat transfer coefficient: 15 W/m^{2}K [16].
- The HTF is assumed to be steady, weakly compressible, and laminar.
- Cross flow between the channel walls does not occur.
- Effect of gravity and viscous dissipation have been ignored.
- The fluid inlet temperature is 25 °C.
- The pressure at the outlet is considered atmospheric.
- The optical concentrator is perfectly aligned to the solar cell and the irradiance profile is not affected by the Fresnel lens temperature.
- Direct normal irradiance (DNI) is 1000 W/m^2, simulating relatively extreme conditions. Light rays are monochromatic, with a wavelength of 660 nm [27].
- Losses caused by nonuniformities in the irradiance profile are insignificant as the peak to average ratio is well below 4 [28,29].
- The parasitic losses for cooling the circulating fluid are excluded
- The energy flux over the receiver is:

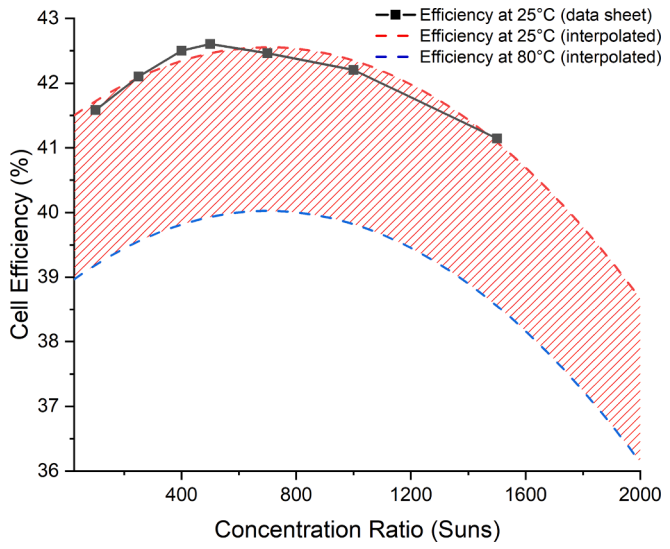

Fig. 3. Cell efficiency as a function of concentration ratio and temperature.

$$P_{opt} = A_{opt} DNI \eta_{opt} \tag{6}$$

Consequently, the input heat rate is:

$$\dot{Q}_{heat} = P_{opt} - P_{sc,elec} \tag{7}$$

Where $P_{sc,elec}$ is found by evaluating the following equation over the mesh of the germanium layer of the solar cell:

$$P_{sc,elec} = P_{opt} \times \eta_{sc} \tag{8}$$

The system performance is evaluated in several ways, after measuring the maximum and minimum solar cell temperature we can find the cell temperature non-uniformity:

$$\Delta T_{sc} = T_{sc,max} - T_{sc,min} \tag{9}$$

The heat sink's thermal resistance (K/W) is calculated as:

$$R_{th} = \frac{T_{sc,max} - T_{f,in}}{\dot{Q}_{heat}} \tag{10}$$

Where a heat sink is preferred to have a low value. Pumping power is estimated as:

$$P_{pump} = \dot{V} \Delta p \tag{11}$$

Net electrical efficiency is evaluated over the germanium layer mesh, multiplying this by the light power volumetrically gives the electrical power produced. The system's net electrical efficiency (which differs from the specific cell electrical efficiency) considers all irradiance incident on the CPV module. This is defined as:

$$\eta_{sys,elec} = \frac{P_{sc,elec} - P_{pump}}{P_{opt}} \tag{12}$$

Thermal power is found by integrating the following equation over the module outlet:

$$\dot{Q}_{th} = \dot{m} c p_f (T_{f,out} - T_{f,in}) \tag{13}$$

By integrating the equation across the outlet, a more accurate value is attained than would be when using the average temperatures. The thermal efficiency is found by:

$$\eta_{th} = \frac{\dot{Q}_{th}}{P_{opt}} \tag{14}$$

Naturally, the total system efficiency (excluding parasitic losses for sun tracking and pumping power outside the cooling system) is:

$$\eta_{sys,tot} = \frac{\dot{Q}_{th} + P_{sc,elec} - P_{pump}}{P_{opt}} \tag{15}$$

Note that this value describes the efficiency of the CPV module based on the irradiance incident on the module surface, hence, the optical efficiency of the concentrator is not included. Similarly, the exergy efficiencies are taken as a percentage of the solar energy incident on the receiver module, rather than the input aperture of the primary optic.

2.3. Method of exergy analysis

Exergy analysis in this study is similar to those feature in [5,8,30,31]. Firstly, solar exergy (where T_s is 6000 K) is defined as:

$$E_{Sun} = C\left[1 - \frac{3}{4}\left(\frac{T_a}{T_s}\right) + \left(\frac{T_a}{T_s}\right)^4\right] \tag{16}$$

Electrical exergy efficiency is therefore:

$$\xi_{Elec} = \frac{P_{Elec} - P_{pump}}{E_{Sun}} \tag{17}$$

Thermal exergy is estimated as:

$$E_{th} = \dot{m} c_{p,f} \left\{ (T_{f,out} - T_{f,in}) - (T_a + 273) ln\left(\frac{T_{f,out} + 273}{T_{f,in} + 273}\right) \right\} \tag{18}$$

It follows that the thermal exergetic efficiency is:

$$\xi_{th} = \frac{E_{th}}{E_{Sun}} \tag{19}$$

Naturally, the total exergetic efficiency is:

$$\xi_{Total} = \xi_{th} + \xi_{Elec} \tag{20}$$

Note that this excludes losses for the optic, such as the transmissivity of the lenses, reflectivity of mirrors or the electricity used for solar tracking.

2.4. Method for optical coupling

Using the COMSOL 5.6 *Ray Optics* package the irradiance distribution of a 21 cm^2 Fresnel lens is incorporated, as well as the irradiance profile of a Fresnel-based UH concentration optic. The geometric concentration ratio of each primary optic's inlet aperture and the solar cell is ~ 1500 suns and ~ 6000 suns respectively. To save on computational power, the optical analysis is done separately on a copper plate. The irradiance applied over the cell represented as a heat source (uniform in cell depth but varying with focal image in × and z axes) where the total energy in this heat flux is the power leftover after electrical power generation. The electrical power is found by applying equation (8) over the active area of the solar cell. By separating these physics packages, the heat over the cell can be generated as a volumetric domain heat source rather than a surface heat flux. The irradiance of the focal spot which misses the cell is added as a surface heat flux.

An alternative focal image based on the measured diameter has been produced using a Gaussian distribution to determine how valid this simplification is, since Gaussian ray distributions have been observed [32]. The power of the concentration (integrated energy flux over area) is the same in each case and is based on the energy flux over the concentrator's exposed surface and its optical efficiency (transmissivity) measured using a spectrophotometer.

Since the physical validation experiment is under a WACOM solar simulator [Model no. WXS-210S-20], we must consider the focal image when the Fresnel lens is illuminated by the divergence angle of sunlight (0.27°) and the solar simulator (1.43°). The resultant optimum focal spots can be seen in Fig. 4A-D, with peak concentrations of 302.17 suns

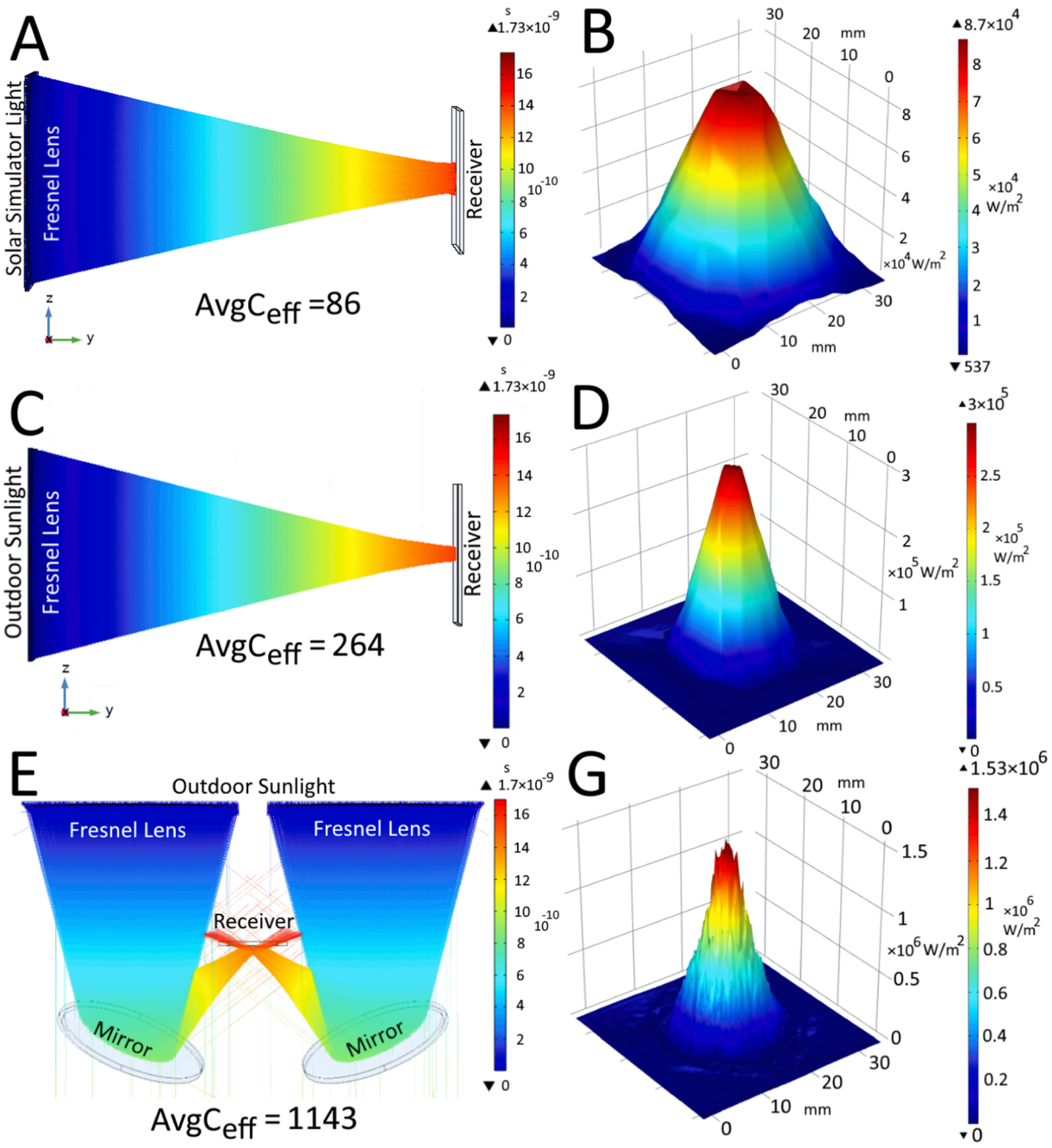

Fig. 4. (A/C) Ray tracing of Fresnel lens focusing to a copper plate using the WACOM solar simulator's divergence angle (1.43°) and the sunlight's divergence angle (0.27°) (B/D) Focal spots generated by each respective divergence angle over an area of 36 mm^2. (E) Ray Tracing of UH-CPV optic (F) focal spot generated by UH-CPV optic.

and 87.06 suns (where 1 sun = 1000 W/m^2) under outdoor and indoor conditions, respectively. Note the outdoor DNI value is fixed at 1000 W/m^2 for the theoretical study. The local concentration ratio feeds into equation (1) to calculate cell efficiency. The diameter of each focal image is 1.2 cm and 2.8 cm respectively. The solar simulator's focal image diameter has been confirmed experimentally. The number of rays released in the model is increased until results stabilise [33]. The number of rays released in Fig. 4A-D and Fig. 4E-F is 110,000 and 500,000, respectively. The light rays are monochromatic with a wavelength of 660 nm, this is used as an approximate average for the wavelengths that produce a spectral response from the MJ solar cell (~300–1800 nm). The cell absorptivity it set to 85% [4] to account for the differences in global and direct irradiance produced by the solar simulator's AM1.5G filter and the light reflected by the cell for wavelengths of 300 nm to 1850 nm. The effective concentration is defined as the average irradiance incident on the active area of the solar cell in suns. Experimentally, this is found using the ratio of short circuit current under concentration, $I_{sc,conc}$, to short circuit current with no concentration, $I_{sc,bare}$:

$$C_{eff} = I_{sc,conc}/I_{sc,bare} \tag{21}$$

There is some error between theoretical and experimental values, as the short circuit current is affected non-linearly by the concentration and by the cell temperature. The UH-CPV optical image is based on a multistage optic which uses 4 of the same Fresnel lenses. These concentrate on to Reflectech mirrors (with a η_{opt} of 87%) which direct

Table 4
Structural properties used in stress analysis.

Layers	Young's modulus (E, GPa)	Poisson ratio (ν)	Coefficient of thermal expansion (α, 1/°C)
Copper	110.0	0.35	1.7×10^{-5}
GaInP, GaInAs, & Ge	102.7	0.28	6.1×10^{-6}

the light to the solar cell. This ray tracing method is conducted in the same way as the previous images under the sun's divergence angle. The maximum concentration ratio generated by this irradiance profile is 1534.10 suns, as seen in Fig. 4E-F. Fig. 4 shows the average C_{eff} based on the concentration ratio of irradiance within the ray tracing model over the solar cell area. The UH-CPV optic is only considered in outdoor conditions. The total η_{opt} is 89% for the single Fresnel lens (for indoor and outdoor conditions), 77.4% for the UH-CPV optic.

2.5. Thermal stress coupling

Using COMSOL 5.6 *Solid Mechanics* package and *Thermal Expansion* Multiphysics, thermal stress is evaluated as in [34,35]. Different materials have different expansion coefficients, thus when heated, physical stress will be generated between different materials. To interpret effect on the lifetime we shall investigate the thermal stresses generated between the cell and the top copper layer of the cell's circuit board. This will be evaluated in terms of the von Mises stress (MPa) where a lower stress is preferrable. The structural properties of the materials in this section of the study are detailed in Table 4.

3. Validation of numerical solution

3.1. Theoretical validation

A mesh independence study has been conducted. The number of mesh elements has been varied to determine how the number of elements affects the solution. This study and the meshed model for the Aluminium SS model are presented in Fig. 5. To balance computational time and solution accuracy, 6.44×10^5 elements was chosen with relatively little error.

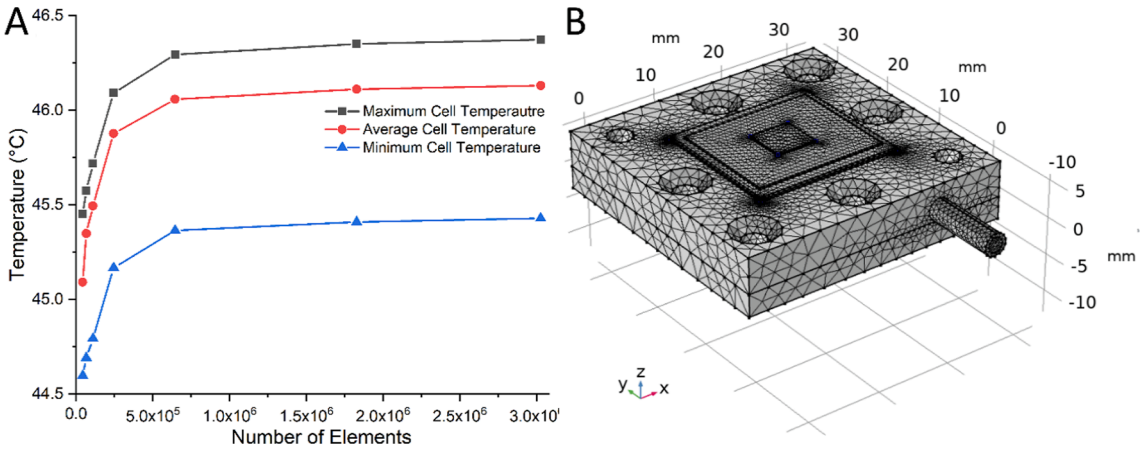

Fig. 5. (A) Mesh independence analysis in terms of solar cell temperature (B) Mesh of single serpentine model using 6.44×10^5 elements.

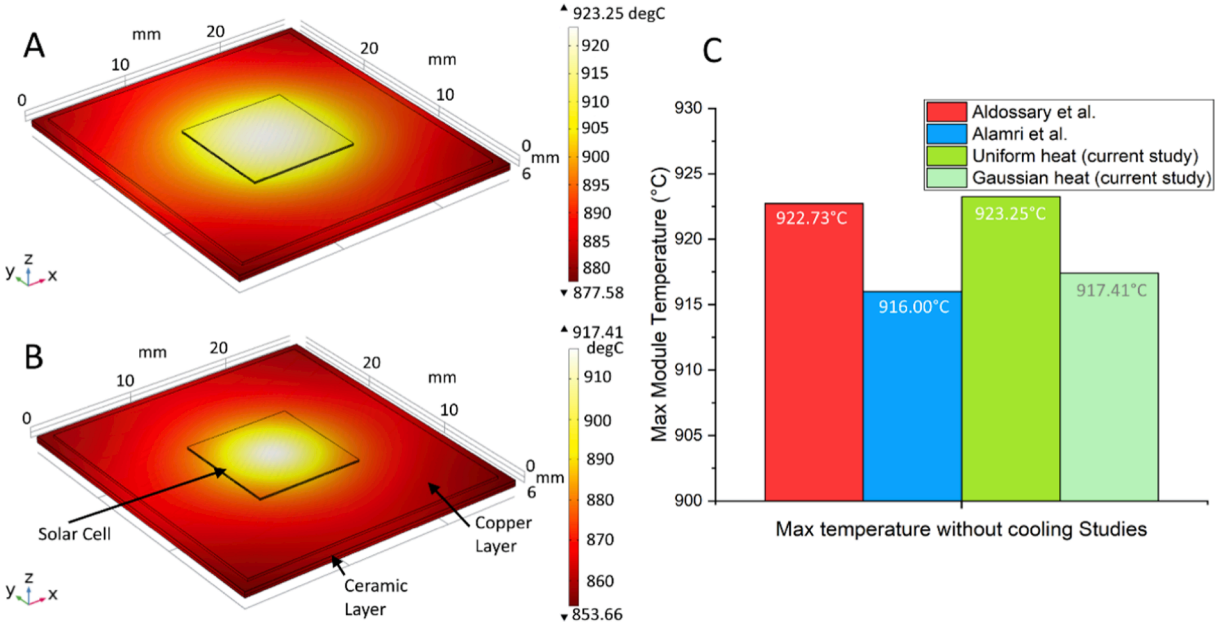

Fig. 6. Predicted temperature profile solar cell with no cooling aid assuming: (A) uniform illumination (B) gaussian illumination. (C) comparison to other studies.

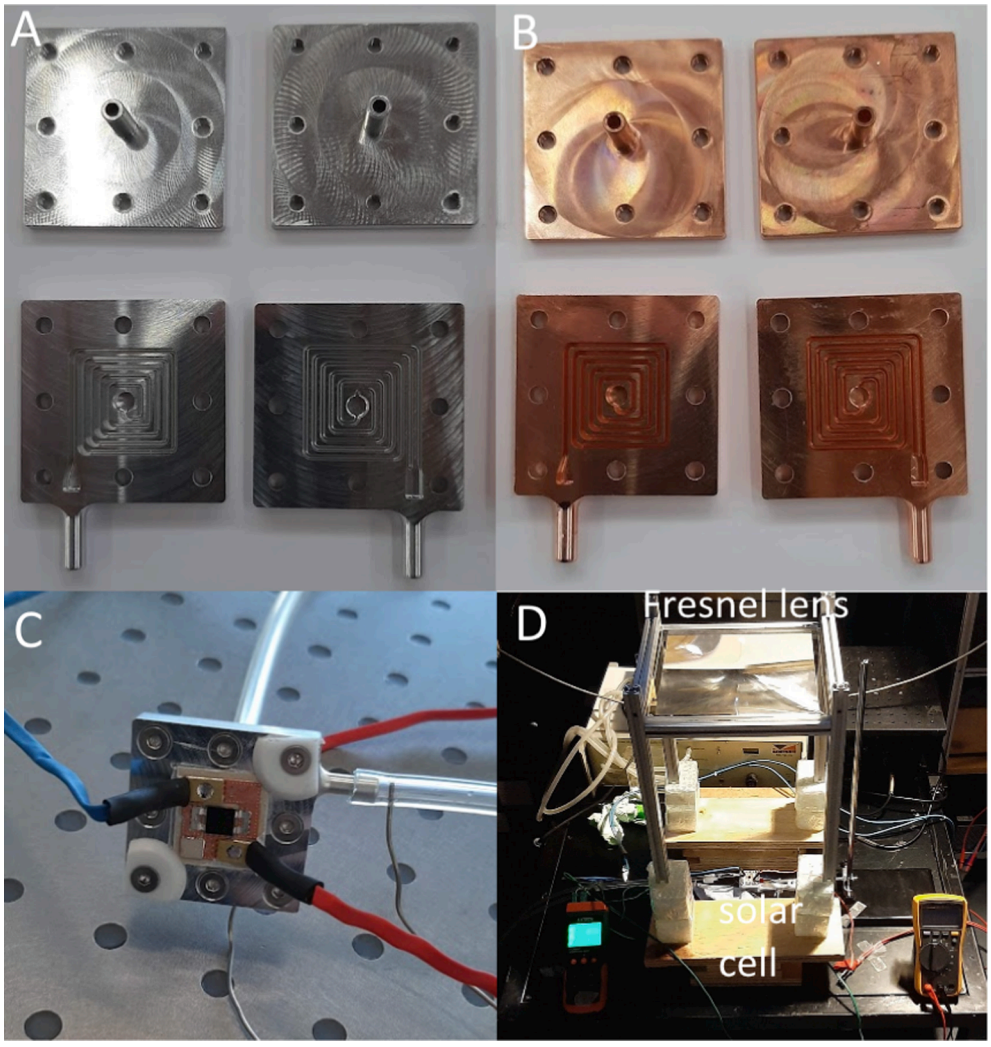

Fig. 7. (A/B) Models of serpentine cooling modules used in physical experiments, from left to right: SS Al, DS Al, SS Cu, DS Cu. (C) CPV module connected to pump and IV tracers with thermocouples (D) testing apparatus underneath WACOM solar simulator.

The focal spot under outdoor conditions has been compared to other theoretical studies for a 10 mm^2 solar cell with no heat sink under a geometric concentration ratio of 500 suns, Aldossary et al. [3] assumes uniform illumination as is standard within the literature, Alamri et al. [7] use COMSOL's *Ray Optics* physics package. As is seen in Fig. 6, good agreement is found when using the same boundary conditions.

3.2. Experimental validation

The serpentine cooling modules under a single Fresnel lens were exposed to a class AAA WACOM solar simulator with a Xenon short-arc lamp with a UV filter and an AM1.5G filter to emulate a solar irradiance approximating 1000 W/m^2. AM1.5D is preferred when evaluating concentrator photovoltaics, hence the factor of 85% has been applied to account for the light scatter [4]. Test samples can be seen in Fig. 7.

A Fluke PTi120 thermal imaging camera was used to find the peak experimental temperatures over the surface of the solar cell, type K thermocouples were used to determine the fluid inlet and outlet temperatures. The uncertainty of these are ± 2% and ± 0.75%, respectively. An EKO mp-160 IV tracer was used to track the maximum power point value with an error of ± 0.5%. To combat the effect of the flicker of the solar simulator arc lamp, several IV tracer measurements were taken and averaged. A likely cause of error is cross flow occurring between the channels, shortening the flow path. This is more likely to occur at higher flow rates due to the added pressure of the fluid. The power loss through wires between the IV tracer and the solar cell contribute to error in the power values, as well as the discrepancy between AM1.5G and AM1.5D. Fig. 8 shows the maximum temperature found through indoor experimentation of each module over a range of flow rates with a comparison to the different simulation models. The maximum error found in the peak cell temperature for the ray trace-based study was 3.17%. The experimental C_{eff} was 82.88 suns, which fits closely to the ray traced image with an average C_{eff} of 85.59 suns. The gaussian method produced an average C_{eff} of 255.78.

Physical validation experiments revealed that while the gaussian distribution of irradiance resulted in relatively accurate values for the temperature profile (with error of ~ 12%), the electrical power output was higher than expected. This is because of the steep shape of the peak; excessive energy is converted into electrical power. Across all Gaussian-based models, the lowest electrical power produced was 2.7 W. For cases where a significant proportion of the light spills past the solar cell, the gaussian irradiance cannot guarantee accurate results, hence ray tracing is recommended for this study. Fig. 9 shows the electrical power produced by the solar cell for each module over a range of flow rates, with comparison to the different simulation models. The maximum error found in the electrical power was 0.37% for the ray trace-based study.

The outlet temperature was lower than the simulation predicted. This is because the simulation considers the module as fully insulated

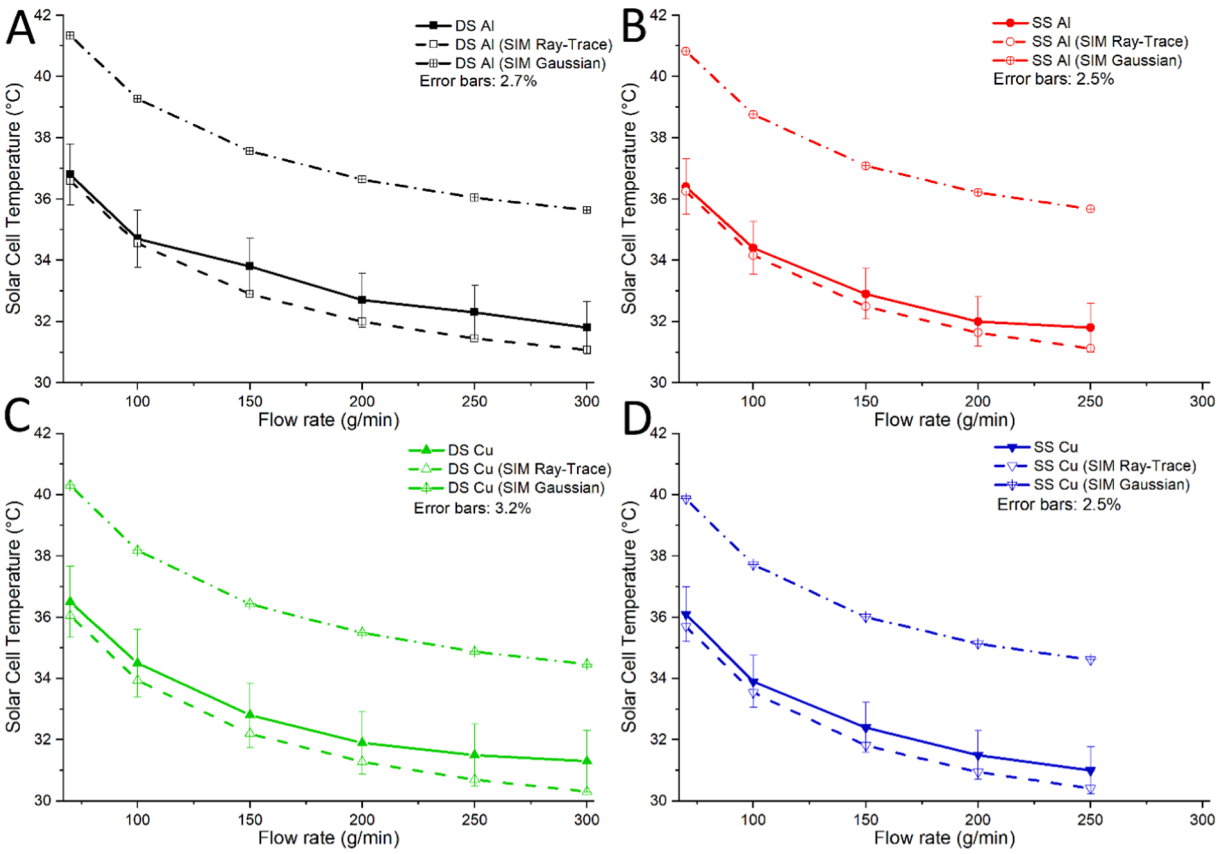

Fig. 8. Maximum cell temperature from indoor experimental analysis and simulation from both ray tracing and Gaussian-based study for (A) Aluminium Double Serpentine (B) Aluminium Single Serpentine (C) Copper Double Serpentine (D) Copper Single Serpentine.

after convection and radiation whereas in reality, there are losses due to conduction, where the module is held by a stand. The simulation results can be tuned using the experimental results. By applying the loss factor in the following equation, the expected experimental outlet temperature can be estimated:

$$T_{f,out} = \{0.0011(\dot{m}) + 0.5158\}\Delta T_f + T_{f,in} \quad (22)$$

Following this tuning, the error is<1% in all cases. The outlet temperature was affected by flow rate and irradiance but was not significantly changed by the specific serpentine geometry or material deployed. Comparison to state-of-the-art CPV systems is based on the current commercial reference point [36,37], key parameters are shown in Table 5.

4. Results and discussion

4.1. Temperature profile of CPV/T module

The temperature profile for aluminium and copper, SS and DS over various flow rates (40–300 g/min) and concentrations are shown in Fig. 10. As expected, the maximum temperature of the solar cell drops sharply with an increase in flow rate, and then only slightly with further increases. The maximum cell temperature is consistently lower in the SS designs for the same flow rate. However, the DS module is not as limited in the maximum achievable flow rate and can therefore achieve a lower maximum cell temperature if needed. Notably, both designs could achieve a maximum volumetric temperature lower than maximum operating temperature (<110 ℃) at the lowest flow rate even at UH irradiance (average C_{eff} of ~ 1150 suns). At higher flow rates recommended operating temperatures were easily reached (<80 ℃), with cell temperature is only slightly higher than the commercial reference (Table 5) for UH conditions. Both the outlet temperature and the temperature nonuniformity are primarily affected by the irradiance incident on the module. The outlet temperature reduces with increased flow rate, as is commonly seen in CPV/T systems, as there is less time for heat transfer to occur. Unexpectedly, the temperature non-uniformity remains more or less stable regardless of flow rate. How this and the maximum temperature of the solar cell affect the thermal stress generated will be discussed in Section 4.4. The temperature distribution was similar across all modules, with a slight shift highlighted by the maximum value. The temperature profile of the aluminium DS module under the UH optic can be seen in Fig. 11.

4.2. Energy efficiency of CPV/T module

Pumping power measures the amount of energy required by the fluid to overcome the pressure drop. This power use will be a parasitic power loss within the CPV/T system. While slightly dependent on the fluid temperature (and hence density), the heat sink geometry is the primary influencer of pumping power. The pumping power for the SS is substantially higher than the DS despite producing only slightly lower values of thermal resistance, highlighted in Fig. 12. This highlights the flaw of the SS design in the substantial pressure drop produced by the long single channel geometry. This also explains why the experimental setup could not achieve a flow rate greater than 250 g/min, as the pressure drop was too great for the pump to overcome. The material choice does not affect pumping power but drawing heat away from the solar cell with a higher thermal conductivity, consistently lead to lower thermal resistances. Thermal resistance was much lower than the commercial reference, this is expected given active cooling is not frequently deployed commercially.

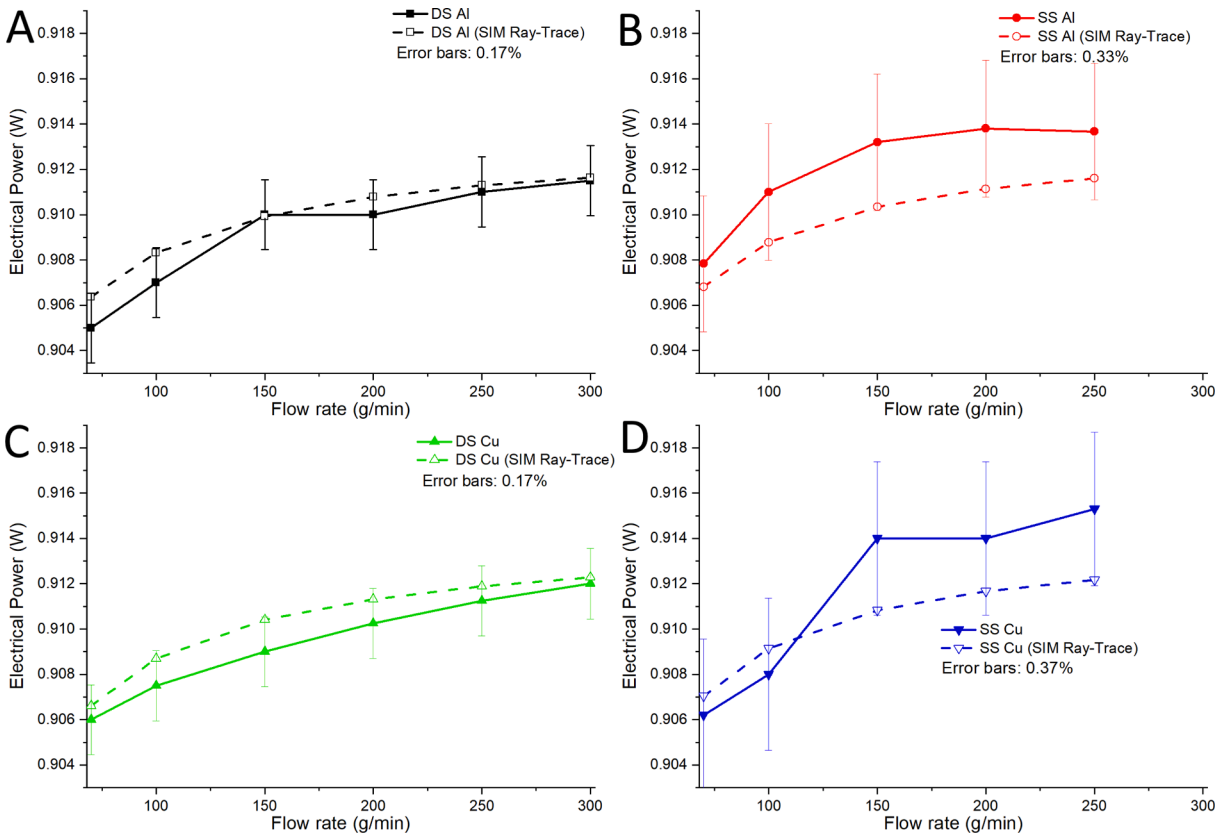

Fig. 9. Electrical power output from solar cell under from indoor experimental analysis and simulation from ray-trace based study for (A) Aluminium Double Serpentine (B) Aluminium Single Serpentine (C) Copper Double Serpentine (D) Copper Single Serpentine.

Table 5
Key parameters of commercial state-of-the-art cpv [36,37].

Parameter	Value
Geometric Concentration Ratio	800
Optical Efficiency	85.0%
R_{th}	9.81 K/W
Operating Cell Temp	60 °C
System Efficiency	36.4%
Cell Efficiency	42.8%

Fig. 13 depicts the efficiencies of the CPV/T modules over various conditions. Specifically, the cell efficiency, the net system electrical efficiency (which differs by including parasitic losses from HTF pumping and optical loss where concentrated light has missed the solar cell's active area), thermal and total system efficiency. As is typically seen in CPV/T systems, higher flow rates led to higher thermal and cell electrical efficiencies. This can be explained by the additional transfer of thermal energy out of the system by the HTF. The detriment of the pumping power is again highlighted in this section. While the solar cell efficiency rises with flow rate, the net electrical efficiency rises and then falls in some cases. This is because, at high flow rates, the additional pumping power to increase flow rate is more than the additional power generated by a lower cell temperature. The SS suffers from this effect more because of its added pressure drop. This effect is more notable at the lower concentration irradiance profile where the temperature of the cell stabilises with lower cooling levels. Since the range of the thermal efficiency is greater, the net electrical power does not detract enough to stop its upward trend. To determine the optimum operation, we must therefore consider the exergetic efficiency. Compared to the commercial reference, the lower cell efficiency can be explained by the effect of higher irradiance levels. This along with the light missing the cell, and the lower optical efficiency brings the net electrical efficiency down. The total efficiency is much higher, showing the benefit of waste heat capture.

4.3. Exergetic efficiency of CPV/T module

Exergetic efficiencies are presented in Fig. 14. Electrically, the trend found is similar to the energy efficiency, where increased flow rates lead to higher electrical exergy efficiency until the added pumping power is greater than the additional electrical exergy gained by further cooling. Again, this effect is more consequential at lower concentrations where the maximum cell temperature is already relatively low. The thermal exergetic efficiency takes the opposite trend to that found in the previous section. With the higher efficiencies found at higher outlet temperatures, the trend found is similar to that found in Fig. 10C. In every case the DS module yields superior performance due to its high performance and relatively low parasitic losses. As has been consistently found throughout, copper is seen to be the superior material for this purpose, owing to its higher thermal conductivity. Given the highest exergetic efficiency is found at the minimum flow rate, one may choose to operate the CPV/T under this condition, where the SS design yields the highest performance. Under UH conditions, achieving a longer lifetime would require higher flow rates to maintain the recommended operating temperature. This would be at a flow rate where the DS design yields a higher exergetic efficiency. Compared to other exergy analyses in the literature, these values are relatively low. These values can be taken as more realistic due to the consideration irradiance distribution, including the light which misses the solar cell. With an assumption of uniform illumination, the exergetic efficiency is expected to be over 30%. Due to the lack of significant difference in cost to manufacture each configuration, the configurations with the highest exergetic efficiencies are expected to be the best performing economically. A full thermo-economic analysis is planned by the authors.

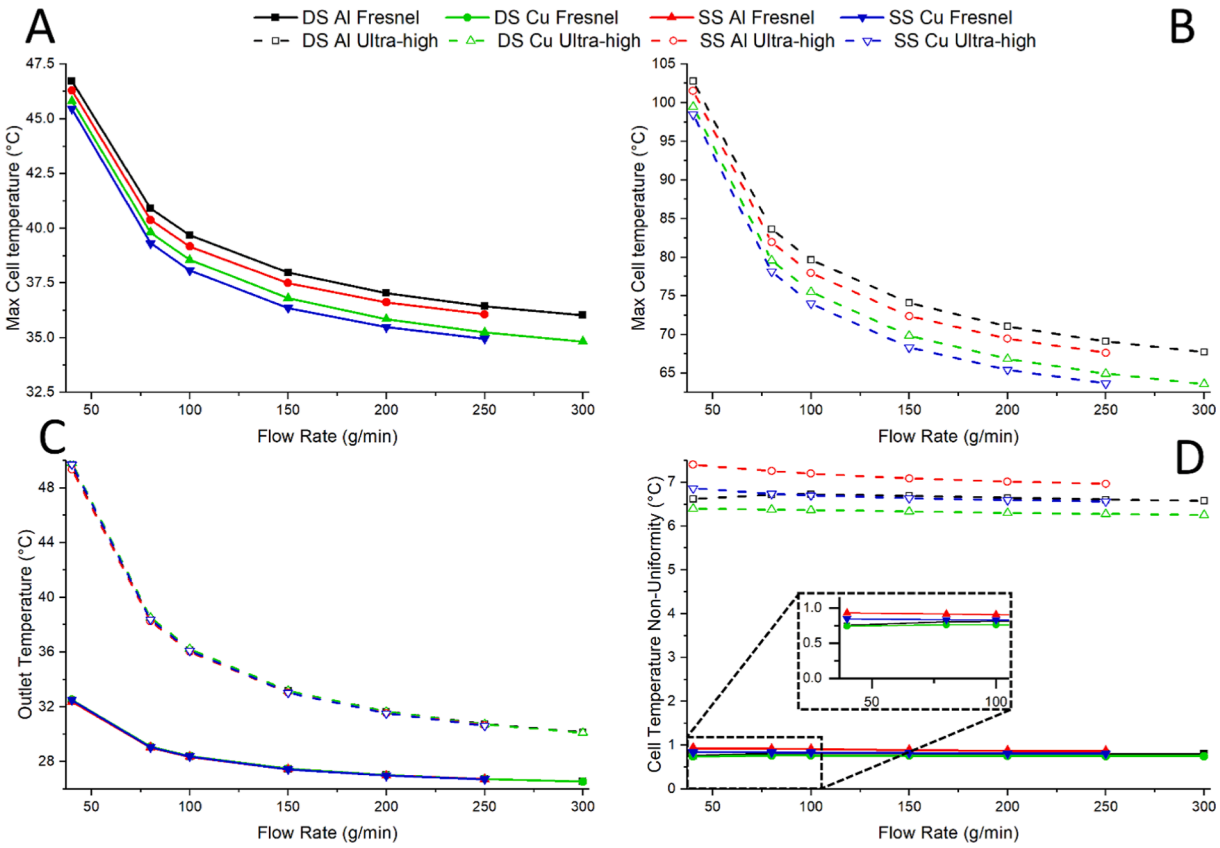

Fig. 10. Temperature profile of each serpentine module over various flow rates: (A) Maximum cell temperature under one outdoor Fresnel lens (B) Maximum cell temperature under UH-CPV optic (C) Fluid outlet temperature under each irradiance profile (D) Cell temperature non-uniformity under each irradiance profile.

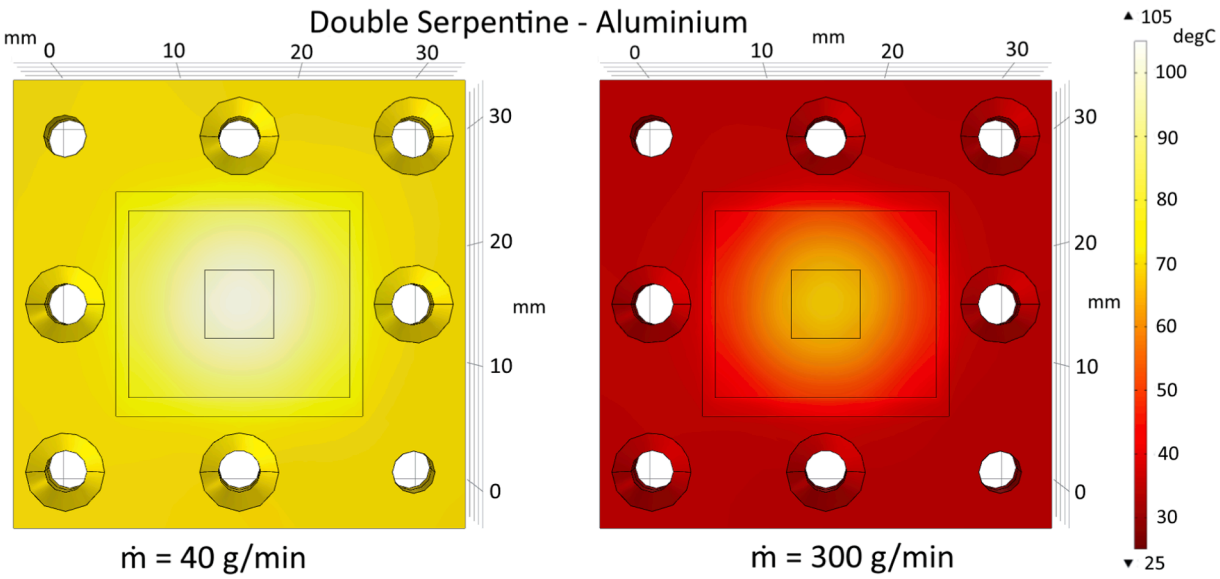

Fig. 11. Surface temperature of the Aluminium DS module at minimum and maximum evaluated flow rate under the UH optic.

4.4. *Thermal stresses*

The peaks of the thermal stress generated within the solar cell are found around the sides, at the boundary between the germanium and copper layers. The profile of the stress generation was similar in every module, with the differences highlighted by the difference in peak value. Fig. 15 shows the distribution of von Mises stress generated between the germanium and top circuit board copper layers for the aluminium DS module.

The trends depicted in Fig. 16, show that the main contributor to the thermal stress generated is the maximum cell temperature. Fig. 10D showed the temperature nonuniformity to vary very slightly in the flow rate, so it is unknown how much this parameter affected the thermal stresses generated. The lowest thermal stress is achieved at the highest

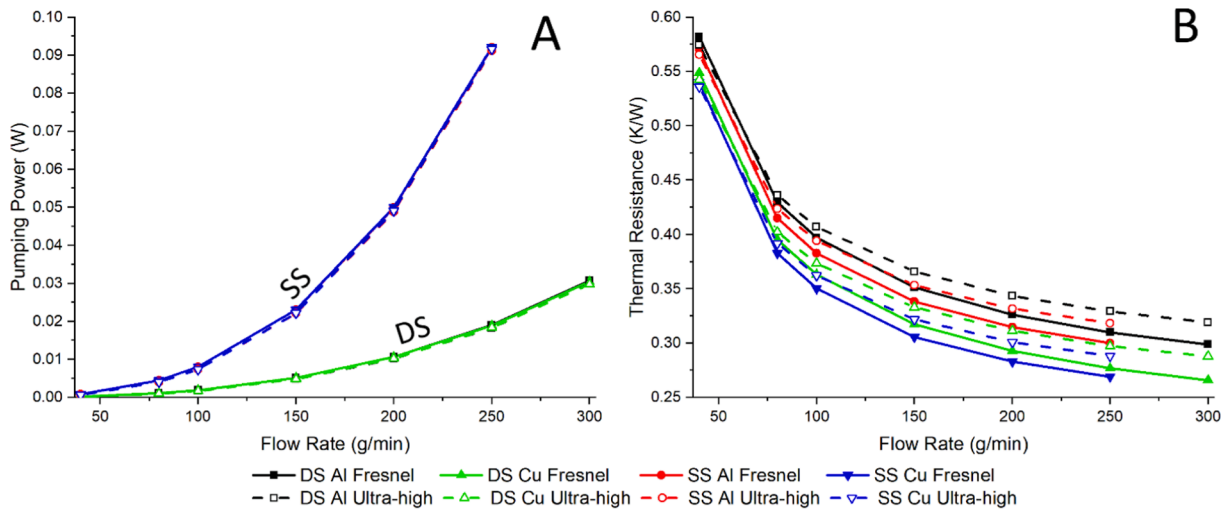

Fig. 12. (A) Pumping power of each serpentine module across flow rate and each irradiance profile (B) Thermal resistance of each serpentine module across flow rate and each irradiance profile.

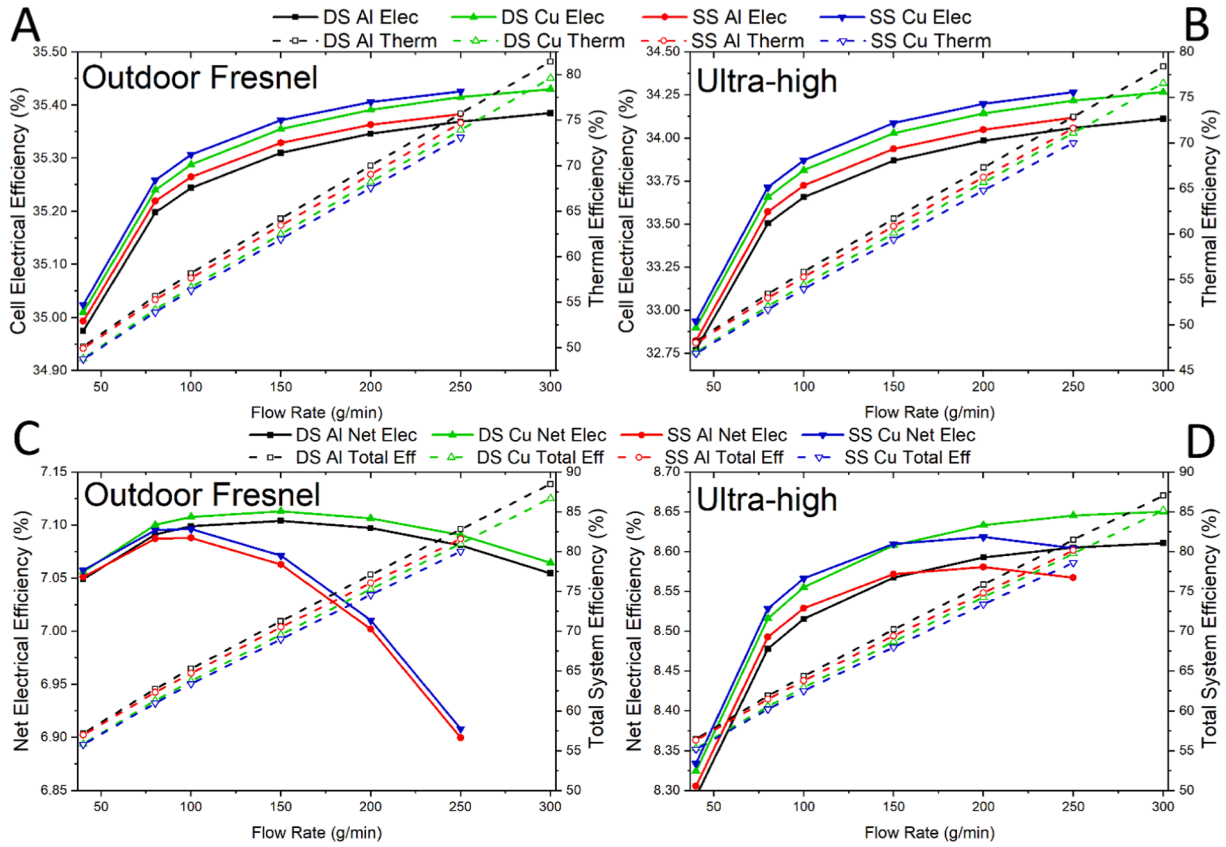

Fig. 13. Solar cell efficiency and thermal efficiency under irradiance profile of (A) Outdoor Fresnel, (B) UH-CPV optic. System net electrical efficiency and the total efficiency for irradiance profile of (C) Outdoor Fresnel, (D) UH-CPV optic.

flow rate, with the copper DS module. When comparing the same flow rates, the SS design leads to a slight reduction in stress because of the lower cell temperature. Unless minimal flow rates are required, recommended operation would be with the DS-based modules.

5. Conclusions

In this study, a novel method of evaluating a CPV/T system is explored and experimentally validated. By considering multiple COMSOL physics packages simultaneously, insights can be gained into all parts of the system. Ray tracing has been used to generate the specific irradiance profiles that the cooling system must be equipped to operate under. Physical validation via extended outdoor experimentation with both optics is the next step of this research. This will add certainty into the method and allow more consideration to non-uniform irradiance and further characterisation of the flow (such as calculating the average Nusselt number). The UH optic shall also incorporate a 4-domed optic to the cell in the hopes of achieving even higher levels of concentration,

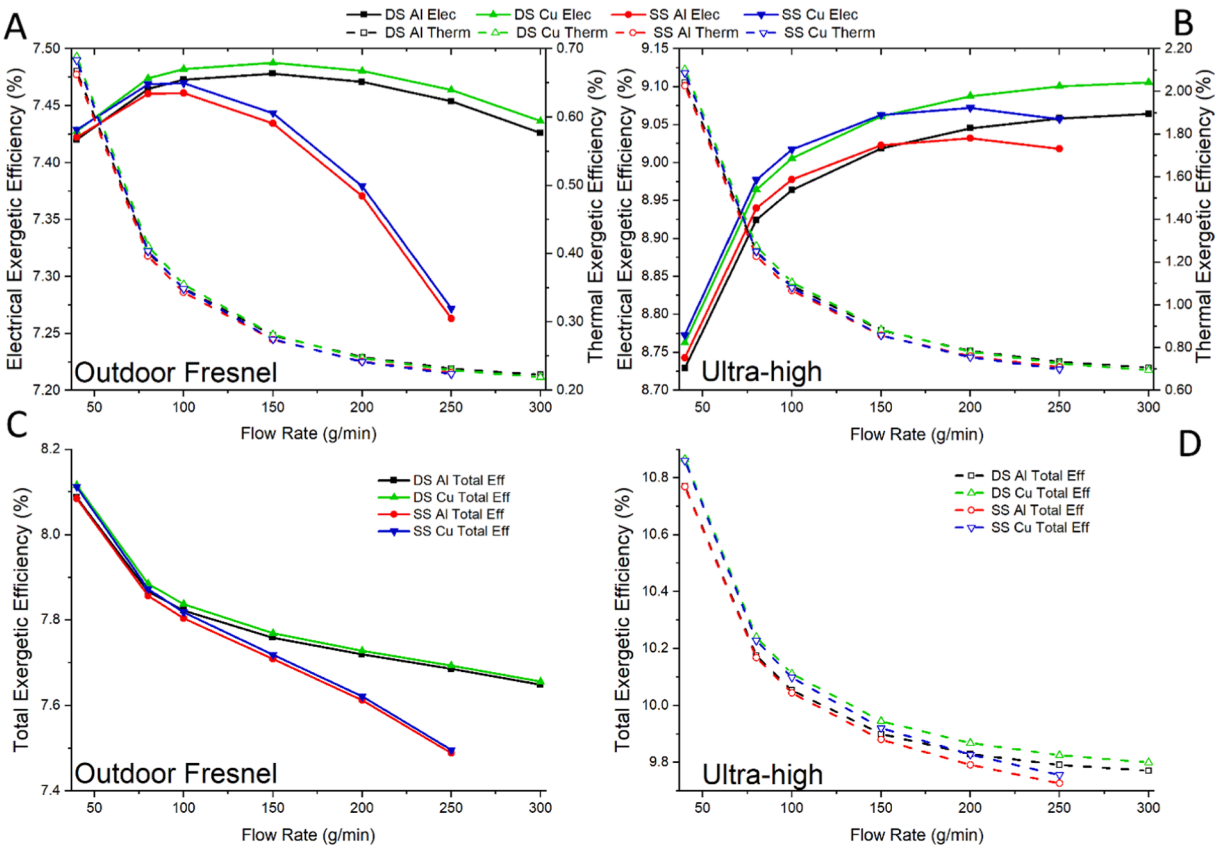

Fig. 14. Electrical and thermal exergetic efficiency of the serpentine modules under irradiance profile of (A) Outdoor Fresnel, (B) UH-CPV optic. Total system exergetic efficiency for irradiance profile of (C) Outdoor Fresnel, (D) UH-CPV optic.

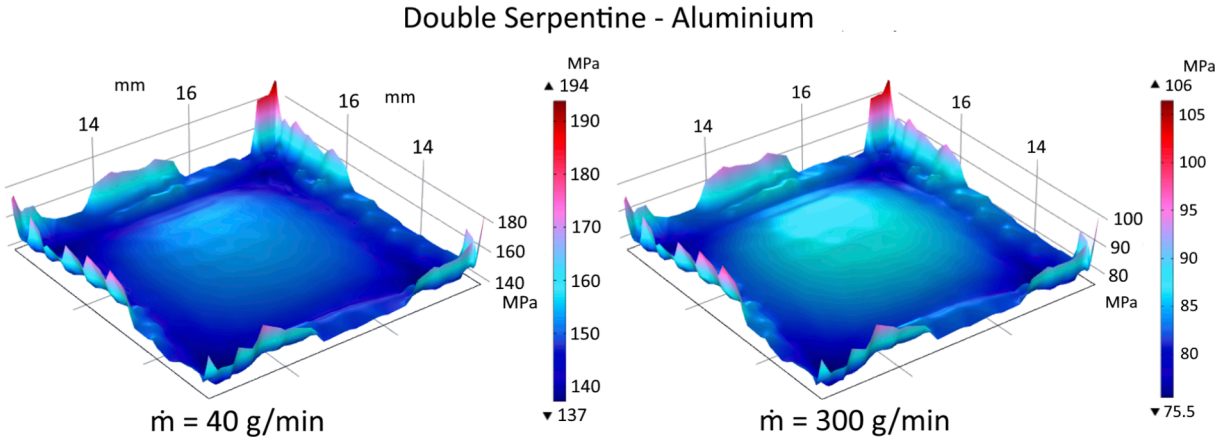

Fig. 15. Distribution of von Mises stress between the germanium layer of the solar cell and the copper layer of the solar cell's circuit board.

testing of which is underway by the authors [38]. The major conclusions are as follows:

- All serpentine-based cooling systems could maintain the UH-CPV/T within recommended operating temperatures.
- The DS design is superior in performance compared to the SS design owing to its low parasitic losses. The SS could only be considered superior if an absolute minimal flow rate is needed or if parasitic losses are not within the system design considerations.
- Copper is a better choice for the heat sink material when compared to aluminium, there was no substantial addition in difficulty for manufacture for these modules. How much the added weight will affect tracking power is yet to be investigated.
- The main contributor to thermal stress is the maximum cell temperature. In this case, cell temperature non-uniformity did not vary heavily under operation changes, so its true influence is uncertain.
- Ray tracing is notably superior in modelling irradiance profiles than Gaussian profiles or uniform heat sources which can substantially overestimate the power and maximum cell temperatures, respectively.

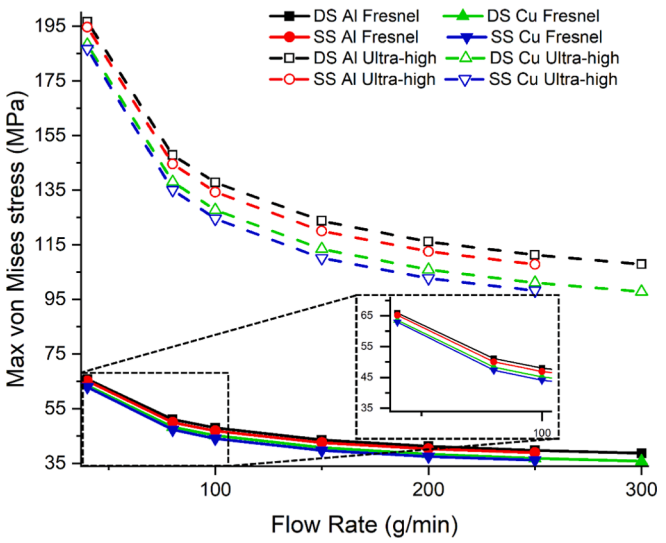

Fig. 16. Maximum von Mises stress found between the copper and germanium layer in the solar cell across flow rate and each irradiance profile.

Declaration of Competing Interest

The authors declare the following financial interests/personal relationships which may be considered as potential competing interests: [William James Cameron reports financial support was provided by Engineering and Physical Sciences Research Council. Mussad Alzahrani reports was provided by Saudi Arabian Cultural Bureau].

Data availability

Data will be made available on request.

Acknowledgments

The UK EPSRC Standard Research Studentship (DTP) supports Mr Cameron. Mr Alzahrani duly acknowledges the financial support from the Saudi Arabia Culture Bureau in the UK.

References

[1] W.J. Cameron, K.S. Reddy, T.K. Mallick, Review of high concentration photovoltaic thermal hybrid systems for highly efficient energy cogeneration, Renew Sustain Energy Rev 163 (2022) 112512, https://doi.org/10.1016/J.RSER.2022.112512.
[2] K. Papis-Frączek K. Sornek A Review on Heat Extraction Devices for CPVT Systems with Active Liquid Cooling Energies 15 17 6123.
[3] A. Aldossary, S. Mahmoud, R. Al-Dadah, Technical feasibility study of passive and active cooling for concentrator PV in harsh environment, Appl Therm Eng 100 (2016) 490–500, https://doi.org/10.1016/J.APPLTHERMALENG.2016.02.023.
[4] M. Cui, N. Chen, X. Yang, Y. Wang, Y. Bai, X. Zhang, Thermal analysis and test for single concentrator solar cells, J Semicond 30 (2009) 44011, https://doi.org/10.1088/1674-4926/30/4/044011.
[5] A. Ahmed, K. Shanks, S. Sundaram, T. Mallick, Energy and exergy analyses of new cooling schemes based on a serpentine configuration for a high concentrator photovoltaic system, Appl Therm Eng 199 (2021) 117528.
[6] Alamri YA, Mahmoud S, Al-Dadah R, Sharma S, Roy JN, Ding Y. Optical Performance of Single Point-Focus Fresnel Lens Concentrator System for Multiple Multi-Junction Solar Cells—A Numerical Study. Energies 2021, Vol 14, Page 4301 2021;14:4301. https://doi.org/10.3390/EN14144301.
[7] Y.A. Alamri, I. Albaik, S. Mahmoud, R. Al-Dadah, M.A. Ismail, Integration of concentrated multi-junction solar cells with small-scale organic rankine cycle, Energy Convers Manag 239 (2021) 114235, https://doi.org/10.1016/J.ENCONMAN.2021.114235.
[8] D. Gao, Y. Zhao, K. Liang, S. He, H. Zhang, H. Chen, Energy and exergy analyses of a low-concentration photovoltaic/thermal module with glass channel, Energy 253 (2022) 124058, https://doi.org/10.1016/J.ENERGY.2022.124058.
[9] H. Hassan, M.S. Yousef, M. Fathy, M.S. Ahmed, Assessment of parabolic trough solar collector assisted solar still at various saline water mediums via energy, exergy, exergoeconomic, and enviroeconomic approaches, Renew Energy 155 (2020) 604–616, https://doi.org/10.1016/J.RENENE.2020.03.126.
[10] E.M. Abo-Zahhad, S. Ookawara, M.F.C. Esmail, A.H. El-Shazly, M.F. Elkady, A. Radwan, Thermal management of high concentrator solar cell using new designs of stepwise varying width microchannel cooling scheme, Appl Therm Eng 172 (2020) 115124, https://doi.org/10.1016/j.applthermaleng.2020.115124.
[11] A.Y.M. Ali, E.M. Abo-Zahhad, A. Radwan, H.I. Elqady, M.F. El-Kady, S. Ookawara, Design and optimization of microchannel heat sink for densely packed high concentration solar cells. ASME,, et al., Heat Transf Summer Conf HT 2020, collocated with ASME 2020 fluids eng div summer meet ASME 2020 18th int conf nanochannels, Microchannels, Minichannels 2020 (2020), https://doi.org/10.1115/HT2020-9097.
[12] E.M. Abo-Zahhad, S. Ookawara, A. Radwan, A.H. El-Shazly, M.F. Elkady, Numerical analyses of hybrid jet impingement/microchannel cooling device for thermal management of high concentrator triple-junction solar cell, Appl Energy 253 (2019) 113538, https://doi.org/10.1016/j.apenergy.2019.113538.
[13] A. Y.M. Ali, E. M. Abo-Zahhad, H.I. Elqady, M. Rabie, M.F. Elkady, S. Ookawara, A. H. El-Shazly, A. Radwan, Thermal analysis of high concentrator photovoltaic module using convergent-divergent microchannel heat sink design, Appl Therm Eng 183 (2021) 116201.
[14] A. Ahmed, K. Shanks, S. Sundaram, T.K. Mallick, Theoretical investigation of the temperature limits of an actively cooled high concentration photovoltaic system, Energies 13 (8) (2020) 1902.
[15] A. Ahmed, G. Zhang, K. Shanks, S. Sundaram, Y. Ding, T. Mallick, Performance evaluation of single multi-junction solar cell for high concentrator photovoltaics using minichannel heat sink with nanofluids, Appl Therm Eng 182 (2021) 115868, https://doi.org/10.1016/j.applthermaleng.2020.115868.
[16] Siyabi I Al, Shanks K, Mallick T, Sundaram S. Thermal analysis of a multi-layer microchannel heat sink for cooling concentrator photovoltaic (CPV) cells. AIP Conf. Proc., vol. 1881, American Institute of Physics Inc.; 2017, p. 070001. https://doi.org/10.1063/1.5001434.
[17] X. Pan, X. Ju, C. Xu, X. Du, Y. Yang, A novel rotational symmetry (RS) connection approach for dense-array concentrator photovoltaic (DA-CPV) modules, Energy Convers Manag 181 (2019) 359–371, https://doi.org/10.1016/j.enconman.2018.12.018.
[18] H. Qandil, Application-based design of the fresnel-lens solar concentrator, AEE World Energy Eng Congr 2019 (6) (2019) 4861–4869, https://doi.org/10.1186/S40807-019-0057-8/TABLES/5.
[19] D. Santos, A. Azgın, J. Castro, D. Kizildag, J. Rigola, B. Tunçel, R. Turan, R. Preßmair, R. Felsberger, A. Buchroithner, Thermal and fluid dynamic optimization of a CPV-T receiver for solar co-generation applications: Numerical modelling and experimental validation, Renew Energy 211 (2023) 87–99.
[20] R. Felsberger, A. Buchroithner, B. Gerl, H. Wegleiter, Conversion and testing of a solar thermal parabolic trough collector for CPV-T application, Conversion and Testing of a Solar Thermal Parabolic Trough Collector for CPV-T Application 13 (22) (2020) 6142.
[21] R.A. Hmouda Y.S. Muzychka X. Duan Experimental and Theoretical Modelling of Concentrating Photovoltaic Thermal System with Ge-Based Multi-Junction Solar Cells Energies 15 11 4056.
[22] M. Deymi-Dashtebayaz, M. Rezapour, M. Farahnak, Modeling of a novel nanofluid-based concentrated photovoltaic thermal system coupled with a heat pump cycle (CPVT-HP), Appl Therm Eng 201 (2022) 117765, https://doi.org/10.1016/J.APPLTHERMALENG.2021.117765.
[23] A. Habchi, B. Hartiti, H. Labrim, S. Fadili, A. Faddouli, N. El hajjam, P. Thevenin, E. Ntsoenzok, Performance study of a new parabolic trough design under optical concentrator effect, Appl Therm Eng 219 (2023) 119500.
[24] AzurSpace., Enhanced fresnel assembly-EFA Type: 3C42A-with 5,5x5,5mm^2 CPV TJ solar cell application: Concentrating photovoltaic (CPV), Modules Typical Average Electrical Data (2014).
[25] K. Shanks, J.P. Ferrer-Rodriguez, E.F. Fernàndez, F. Almonacid, P. Pérez-Higueras, S. Senthilarasu, et al., A >3000 suns high concentrator photovoltaic design based on multiple Fresnel lens primaries focusing to one central solar cell, Sol Energy 169 (2018) 457–467, https://doi.org/10.1016/J.SOLENER.2018.05.016.
[26] T.L. Chou, Z.H. Shih, H.F. Hong, C.N. Han, K.N. Chiang, Thermal performance assessment and validation of high-concentration photovoltaic solar cell module, IEEE Trans Components, Packag Manuf Technol 2 (2012) 578–586, https://doi.org/10.1109/TCPMT.2011.2181165.
[27] L.M. Almara, Ray Optics and Heat Transfer Analysis of a Curved Fresnel Lens Heater for a Desalination System, COMSOL Conf, North America, 2020.
[28] R. Herrero, M. Victoria, C. Domínguez, Understanding causes and effects of non-uniform light distributions on multi-junction solar cells: Procedures for estimating efficiency losses 1679 (2015) 50006, https://doi.org/10.1063/1.4931527.
[29] R. Herrero, M. Victoria, C. Domínguez, S. Askins, I. Antón, G. Sala, Concentration photovoltaic optical system irradiance distribution measurements and its effect on multi-junction solar cells, Prog Photovoltaics Res Appl 20 (2012) 423–430, https://doi.org/10.1002/pip.1145.
[30] G.N. Tiwari, M. Meraj, M.E. Khan, Exergy analysis of N-photovoltaic thermal-compound parabolic concentrator (N-PVT-CPC) collector for constant collection temperature for vapor absorption refrigeration (VAR) system, Sol Energy 173 (2018) 1032–1042, https://doi.org/10.1016/J.SOLENER.2018.08.031.
[31] G. Evola, L. Marletta, Exergy and thermoeconomic optimization of a water-cooled glazed hybrid photovoltaic/thermal (PVT) collector, Sol Energy 107 (2014) 12–25, https://doi.org/10.1016/J.SOLENER.2014.05.041.
[32] J.M. Saura, E.F. Fernández, F.M. Almonacid, D. Chemisana, Characterisation and impact of non-uniformity on multi-junction solar cells (MJSC) caused by concentrator optics, AIP Conf Proc 2149 (2019) 020004, https://doi.org/10.1063/1.5124174.
[33] Comsol. The Ray Optics Module User's Guide 2020.

[34] L. Micheli, S. Senthilarasu, K.S. Reddy, T.K. Mallick, Applicability of silicon micro-finned heat sinks for 500× concentrating photovoltaics systems, J Mater Sci 50 (2015) 5378–5388, https://doi.org/10.1007/S10853-015-9065-2.
[35] Y. Ota, K. Nishioka, Estimation of thermal stress in concentrator cells using structural mechanics simulation, AIP Conf Proc 1616 (2015) 25, https://doi.org/10.1063/1.4897020.
[36] P. Pérez-Higueras, J.P. Ferrer-Rodríguez, F. Almonacid, E.F. Fernández, Efficiency and acceptance angle of High Concentrator Photovoltaic modules: Current status and indoor measurements, Renew Sustain Energy Rev 94 (2018) 143–153, https://doi.org/10.1016/J.RSER.2018.06.011.
[37] P.M. Rodrigo, A. Valera, E.F. Fernández, F.M. Almonacid, Performance and economic limits of passively cooled hybrid thermoelectric generator-concentrator photovoltaic modules, Appl Energy 238 (2019) 1150–1162, https://doi.org/10.1016/J.APENERGY.2019.01.132.
[38] W.J. Cameron, M. Alzahrani, K. Shanks, T.K. Mallick, K.S. Reddy, Optical losses and durability of 4-domed optic for concentrator photovoltaics, Sol. Energy Soc. 16th Photovolt. Sci. Appl. Technol. Conf., University of Salford (2022).